Green Chemistry

Biobased and Degradable Thiol-Ene Networks from Levoglucosan for Sustainable 3D Printing

Journal:	*Green Chemistry*
Manuscript ID	GC-ART-11-2022-004185.R1
Article Type:	Paper
Date Submitted by the Author:	02-Jan-2023
Complete List of Authors:	Porwal, Mayuri; University of Minnesota, Department of Chemical Engineering and Materials Science Hausladen, Matthew; University of Minnesota, Department of Chemical Engineering and Materials Science Ellison, Christopher; University of Minnesota, Department of Chemical Engineering and Materials Science Reineke, Theresa; University of Minnesota, Department of Chemistry

Biobased and Degradable Thiol-Ene Networks from Levoglucosan for Sustainable 3D Printing

Mayuri K. Porwal[a], Matthew M. Hausladen[a], Christopher J. Ellison[a]*, Theresa M. Reineke[b]*

[a] Department of Chemical Engineering and Materials Science, University of Minnesota, Minneapolis, Minnesota 55455, United States

[b] Department of Chemistry, University of Minnesota, Minneapolis, Minnesota 55455, United States

Email: porwa001@umn.edu

*Corresponding authors

Email: cellison@umn.edu, treineke@umn.edu

Abstract

Levoglucosan is a renewable chemical obtained in high yields from pyrolysis of cellulosic biomass, which offers rich functionality for synthetic modification and crosslinking. Here, we report the facile and scalable synthesis of a family of biobased networks from triallyl levoglucosan and multifunctional thiols via UV-initiated thiol-ene click chemistry. The multifunctional thiols utilized in this study can also be sourced from renewable feedstocks, leading to overall high bio-based content of the synthesized levoglucosan networks. The thermomechanical and hydrolytic degradation properties of the resultant networks are tailored based on the type and stoichiometric ratio of thiol crosslinker employed. The Young's modulus and glass transition temperature of levoglucosan-based networks is tunable over the wide range of 3.3 MPa to 14.5 MPa and −19.4 ℃ to 6.9 ℃, respectively. The levoglucosan-based thermosets exhibit excellent thermal stability with $T_{d,10\%}$ > 305 ℃ for all networks. The suitability of these resin formulations for extrusion-based 3D printing was demonstrated using a UV-assisted direct ink write (DIW) system creating 3D printed parts with excellent fidelity. Hydrolytic degradation of these 3D printed parts via ester hydrolysis demonstrated that levoglucosan-based resins are excellent candidates for sustainable rapid prototyping and mass production applications. Overall, this work displays the utility of levoglucosan as a renewable platform chemical that enables access to tailored thermosets important in applications ranging from 3D printing to biomaterials.

Keywords

Levoglucosan, thiol-ene click chemistry, thermosets, 3D printing, DIW, degradable, renewable

1. Introduction

Thermosets are chemically crosslinked materials widely used in applications ranging from foams, coatings, adhesives, and composites to biomedical devices owing to their superior thermal and chemical resistance as well as dimensional stability compared to thermoplastics.[1,2] Nevertheless, the usage of fossil feedstocks for thermoset synthesis and the landfilling of thermoset waste has led to growing environmental concerns.[2] To combat these issues, several biomass-derived feedstocks such as sucrose,[3] trehalose,[4] isosorbide,[5,6] magnolol,[7] itaconic acid,[8–11] and eugenol[12–17] are increasingly being incorporated in various types of thermosetting resins. Concurrently, the use of thiol-ene click chemistry to incorporate these biobased feedstocks into thermosets is becoming prevalent due to the desirable features of the click reaction such as quantitative yields, rapid reaction rates, amenability to ambient conditions, and a library of commercially available thiols.[18] Although the above reported biobased thermosets exhibit a breadth of thermomechanical properties, the suitability of the thermoset for specific applications is usually not demonstrated.[3,10–13,15,17] Additionally, complete functionalization of carbohydrates such as sucrose and trehalose to achieve high functionality crosslinkers is difficult,[3,4] and in cases of feedstocks such as itaconic acid and eugenol, multi-step synthesis may be required to increase the number of reactive functional groups.[10,12]

An important application area for thermosets that has recently emerged is three-dimensional printing (3D printing), which is a vital tool in the fields of biomaterials, rapid visual prototyping, automotive and aerospace materials, flexible robots, and electronics.[19,20] Many of the common polymer 3D printing techniques generate non-degradable thermosetting materials, and some are being increasingly used for mass production instead of prototyping, further worsening the plastic

pollution problem. To mitigate the production and accumulation of 3D printed plastic waste, it is crucial that 3D printing resins that are both renewably sourced and degradable are developed.[19] Renewable feedstocks such as natural phenolics (eugenol, vanillin, guaiacol),[21] succinic and itaconic acid,[22] glycerol,[23] and vegetable oils,[24] have been used to create 3D printing resins via acrylation, typically resulting in nondegradable carbon-carbon bond backbones after free-radical crosslinking. Due to its many advantages, thiol-ene photopolymerization is also gradually being explored in additive manufacturing resins.[25–29] For example, Weems *et. al.* employed naturally sourced terpenes such as linalool, limonene, and β-myrcene to synthesize a variety of photopolymerizable resins that were successfully 3D printed into porous scaffolds with a commercial tetra-functional thiol crosslinker.[28,29] The 3D printing techniques most commonly utilized to print the above reported biobased thermosets are vat photopolymerization systems such as digital light processing (DLP) and stereolithography (SLA).

Direct ink writing (DIW) is an extrusion-based ambient temperature 3D printing technique commonly used for the fabrication of soft robotics, biomaterials, composites, pastes, etc.[20,30,31] As compared to SLA/DLP type 3D printers, which generally require a relatively large amount of resin for printing, DIW printers only require enough resin for the end-product.[24,32] Low printing resin volume is particularly beneficial for material development and is also amenable to the translation of laboratory scale synthesized biobased resins to commercial 3D printing.[24] Moreover, low printing resin volume can help reduce the amount of 3D printing waste since partial curing of the photopolymer in the resin tank can occur in SLA/DLP type printers, thereby often requiring the use of fresh resin for consistent properties. In addition, DIW has low equipment cost and can also be easily used for multi-material printing, allowing for the fabrication of composites and materials with highly tunable properties.[30,33,34] Despite its advantages, DIW has received considerably less

attention in the sustainable 3D printing field, particularly with resins that utilize thiol-ene photopolymerization chemistry.

A biobased feedstock that has been underdeveloped for the synthesis of renewable linear polymers and thermosets is levoglucosan. Levoglucosan is an anhydrosugar obtained as the primary product from the fast pyrolysis of cellulosic biomass (Fig. 1A), in yields as high as 80%.[35] Techno-economic analyses indicate that levoglucosan could be produced from biomass at a low cost of $1.33-3.00 per kg, which is competitive with petroleum-derived feedstocks.[36,37] Levoglucosan is an attractive feedstock for the synthesis of thermosets as it offers rich functionality due to its three hydroxyl groups which can be synthetically modified to obtain tri or higher functionality crosslinkers. In our first work on levoglucosan, we identified mild functionalization routes to access a triallyl levoglucosan monomer, which could be polymerized with biocompatible catalysts to obtain a high functionality allylic scaffold.[38] The levoglucosan based allylic polymer was readily subjected to UV-mediated thiol-ene click chemistry to afford functional polymers with tunable properties and high thermal stability due to the rigid glucopyranose ring in the polymer backbone.[38] While our previous work lays the foundation for reactive levoglucosan based materials, there is still ample space for the development and characterization of levoglucosan-based thermosets. To the best of our knowledge, research on UV-assisted 3D printing of levoglucosan-based resins has not been conducted before. Taken together, these factors have led us to develop levoglucosan-based thiol-ene networks for use as sustainable resins in DIW.

In this study, we present the scalable synthesis of a family of triallyl levoglucosan based thiol-ene networks with four different commercially-available multifunctional thiol comonomers through photoinitiated thiol-ene chemistry (Fig. 1). The fundamental thiol-ene

photopolymerization kinetics were monitored through real-time Fourier-transform infrared (RT-FTIR) spectroscopy. The thermomechanical and degradation properties of the biobased, tunable

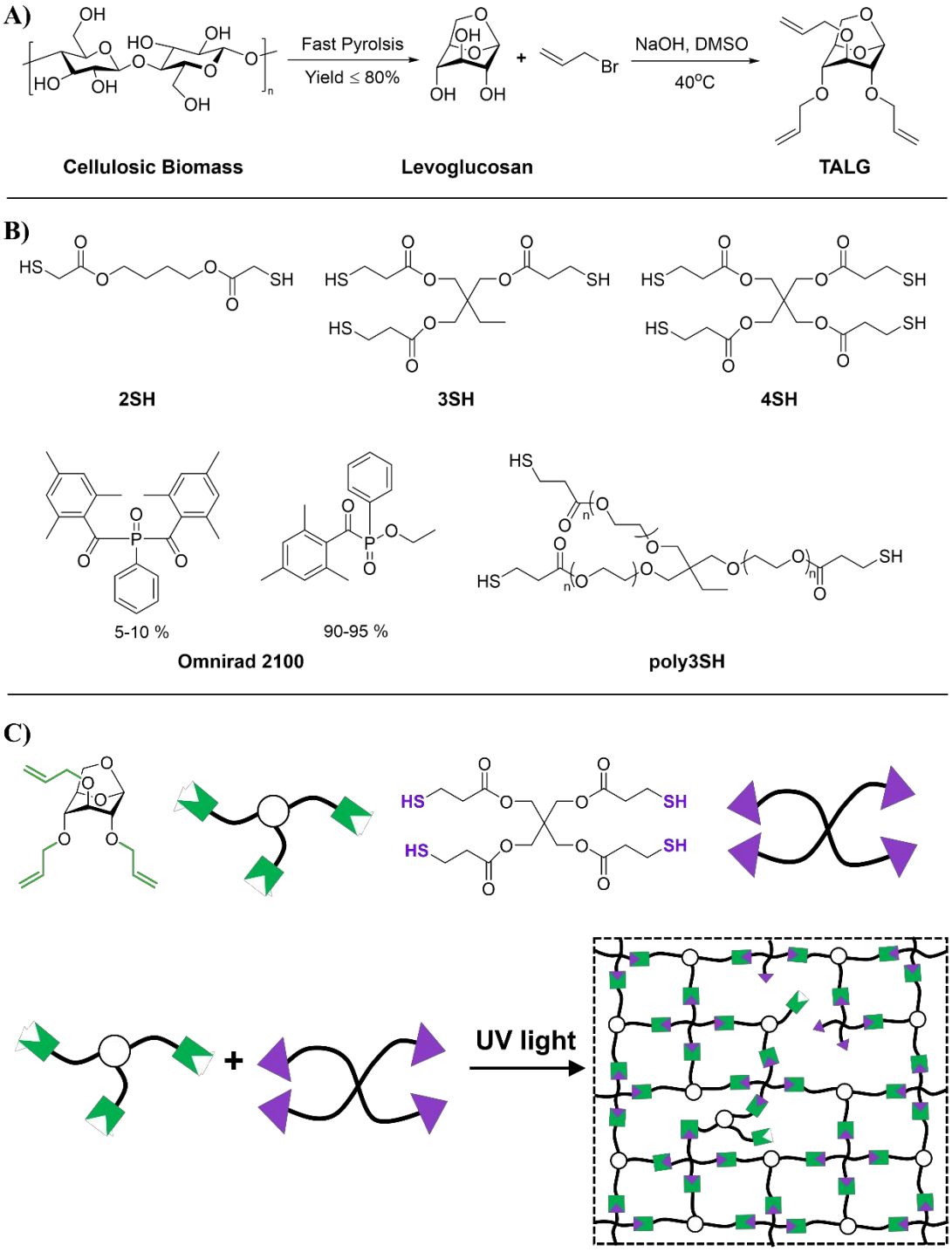

Figure 1 A) Schematic depicting synthesis of levoglucosan from cellulosic biomass.[35] Functionalization of levoglucosan to obtain triallyl levoglucosan (TALG). B) Chemical structures of thiols and photoinitiator. C) Schematic illustration for network formation by thiol-ene photopolymerization of triene and tetrathiol monomers.

thermosets were thoroughly characterized using bulk film samples, and the thermoset structure-property-degradability relationship was elucidated based on the type and stoichiometric ratio of thiol crosslinker employed. The suitability of levoglucosan-based thiol-ene resins for extrusion-based 3D printing technology was demonstrated using an in-house custom-built DIW system. Finally, the hydrolytic degradability of the 3D printed objects was demonstrated, and this property is particularly valuable for rapid visual prototyping and mass production applications. For example, 3D printed prototypes have a much shorter lifetime than structural or biomedical materials, and hence the incorporation of renewable feedstock and degradable linkages in 3D printing resins intended for prototyping will help mitigate 3D printed plastic waste. This work paves the way for further development of levoglucosan as a renewable platform chemical that can be incorporated into a variety of tailored thermosets for 3D printing, coatings, adhesives, and biomedical applications.

1. Experimental Section

2.1 Materials

Levoglucosan was purchased from Biosynth Carbosynth. Sodium hydroxide (NaOH) was purchased from Fisher Scientific, and allyl bromide was obtained from Sigma-Aldrich. All solvents were purchased from commercial sources and used without additional purification. Photoinitiator Omnirad 2100 (mixture of 90−95% ethyl(2,4,6-trimethylbenzoyl)phenylphosphinate and 5−10% phenylbis(2,4,6-trimethylbenzoyl)phosphine

oxide) was generously provided by IGM Resins. 1,4-butanediol bis(thioglycolate) was bought from TCI chemicals, trimethylolpropane tris(3-mercaptopropionate) and pentaerythritol tetrakis(3-mercaptopropionate) were obtained from Sigma-Aldrich. Ethoxylated trimethylolpropane tris(3-mercaptopropionate) or Thiocure 332 was generously provided by Bruno Bock Thiochemicals. The synthesis of triallyl levoglucosan (TALG) is described in a previous report.[38] Fumed silica (FS) rheology control additive Aerosil® 300 was kindly donated by Evonik for modification of resins for 3D printing. To prepare artificial seawater, 24.53 g NaCl, 5.20 g $MgCl_2$, 4.09 g $Na2SO_4$, 1.16 g $CaCl_2$, 0.695 g KCl, 0.201 g $NaHCO_3$, and 0.101 g KBr was combined with 1 L of DI water.

2.2 Representative Thiol-Ene Photopolymerization of TALG

TALG, desired thiol, Omnirad 2100, and ethyl acetate (Table 1) were weighed into a 5 ml scintillation vial and mixed using a vortex device for 5 min to ensure solution homogeneity. The amount of TALG and thiols was calculated to target either 1 : 1 or 0.5 : 1 thiol to alkene end-group ratio (Table 1). Subsequently, the thiol-ene mixture was pipetted into silicone dog-bone molds (gauge dimensions of 2.7 mm x 10.5 mm x 0.9 mm (W x L x T)) and cured using an OmniCure S1500 Spot UV Light Curing System (Excelitas Technologies, broad spectral range of 320-500 nm). Samples were irradiated at an intensity of 100 mW/cm^2 for 7.5 mins, then flipped over, and exposed for an additional 7.5 mins. The cured thermosets were dried under vacuum overnight at room temperature to remove any residual ethyl acetate prior to characterization. **2.3 Hydrolytic Degradation of Thiol-Ene Networks**

Dog-bone specimens post tensile testing were used as samples to investigate the hydrolytic degradation of thiol-ene networks. The samples were weighed to get an initial mass and then dispensed into 20 ml scintillation vials. Each sample was then loaded with 10 ml of 0.1 M NaOH, 0.5 M NaOH, 1 M NaOH, 0.1 M NaOH/THF (water/THF (v/v) = 1 : 1), or 0.1 M NaOH/Acetone

(water/acetone (v/v) = 1 : 1) solutions to start the degradation test. The samples were gently mixed with a benchtop platform shaker at room temperature. After 1 week, the samples were decanted, dried by blotting with Kimwipe, and then dried overnight in a vacuum oven with gentle heating (40 – 50 ℃). The samples were immediately weighed after drying to record mass loss due to hydrolysis. Samples were then re-immersed in the original degradation solution to continue the hydrolysis.

2.4 Hydrolytic Degradation of 3D Printed Parts

To investigate the hydrolysis of the 3D printed parts, the 3D printed leaves were first dispensed into four small beakers. Each sample was then loaded with 10 ml of 1 M NaOH, 1M HCl, de-ionized water, or artificial seawater and left at room temperature. The entire hydrolysis process was continuously monitored by taking photographs of the sample.

2.5 Characterization

A Bruker Avance III HD 400 spectrometer at the University of Minnesota Twin Cities was used to obtain all NMR spectra in either deuterated chloroform ($CDCl_3$) or deuterated water (D_2O). The thiol-ene curing kinetics were studied via RT-FTIR using a Thermo Fisher Scientific Nicolet 6700 FTIR spectrometer with a KBr beam splitter and an MCT-A detector (Thermo Fisher Scientific, Waltham, MA). A drop of the freshly prepared monomer mixture containing TALG, thiol, and Omnirad 2100 was sandwiched between two polished NaCl plates. The monomer mixtures were irradiated using a UV light source (OmniCure S1500 Spot UV Light Curing System, Excelitas Technologies) at an intensity of 50 mW/cm^2. Upon UV irradiation, spectra were recorded every 36 ms at an average of 1 scan with a spectral resolution of 16 cm^{-1} for a total of 300 s. Tensile testing was performed on a Shimadzu AGS-X with dogbone shaped samples with the approximate gauge dimensions, 2.7 mm x 10.5 mm x 0.9 mm (W x L x T). The tensile samples

were extended at 5 mm/min and 6 replicate runs were averaged. Thermogravimetric analyses were performed on a TA Instruments Q500 under nitrogen atmosphere at a heating rate of 10 °C min^{-1}. The thermal properties of the thermosets were characterized using a Mettler Toledo DSC1 instrument under nitrogen atmosphere at a heating rate of 10 °C min^{-1}. The second heating curve was used for glass transition temperature (T_g) analysis to erase any thermal history. Dynamic mechanical analysis (DMA) was performed with an RSA-G2 solid analyzer (TA instruments) equipped with a tensile clamp. Storage modulus and tan δ data of the thermosets was measured by applying a frequency of 1 Hz and a strain of 0.05% at a temperature ramp rate of 5 ℃/min. Rheological experiments were conducted using a DHR-3 rheometer (TA Instruments). For liquid samples (TALG, TALG and thiols, etc.), experiments were performed with a 40 mm parallel plate geometry and for the printing resin, a 25 mm parallel plate geometry was used, with gaps between 250 and 350 μm typically employed. Steady shear experiments were conducted from 0.01 to 1000 Hz and oscillatory amplitude sweeps were performed at 1 Hz. The measured shear stress data from steady shear experiments with parallel plates was corrected for non-Newtonian samples using the Weissenberg-Rabinowitsch equation:[39]

$$\sigma_R = \frac{2M}{\pi R^3}\left[\frac{3}{4} + \frac{1}{4}\frac{d\ ln(M)}{d\ ln(\dot{\gamma})}\right] \quad (1)$$

2.6 3D printing

To prepare the resin for printing, TALG and poly3SH were mixed to target a 1 : 1 thiol to alkene end-group ratio, and the desired amount of Omnirad 2100 (4 wt% or 5 phr) was added to the mixture. No ethyl acetate diluent was added to the 3D printing resin formulation. The TALG-poly3SH mixture was then mixed by hand with 12-14 wt.% fumed silica to generate a yield stress material with suitable stability for printing. This resin was placed in a 10cc syringe (Nordson EFD) and centrifuged for a total of 7 minutes at 3,500 rpm in a ThermoFisher centrifuge to degas the

resin. Resins were printed on a custom, in-house built direct ink write system consisting of a 3-axis gantry and positioning system (modified Stratasys Dimension 768) with a linear actuator for dispensing the resin. G-code was generated using the Slic3r software and operation of the printer was executed using Repetier software. All prints were conducted at a print speed of 10 mm/s, using a plastic tapered tip (Nordson EFD) with a 400μm diameter and using 200 μm layer heights. After completion of the printing of a layer, the gantry system would move the printhead, such that the printed part was exposed to a UV light source (OmniCure S1500 Spot UV Light Curing System, Excelitas Technologies) for 10 seconds, with a light intensity of 25 mW/cm^2. The printing resin was deposited onto a Teflon sheet lined glass build plate at room temperature. After completion of the printing process, the printed parts were post-cured for 60 seconds at room temperature with a UV light intensity of 25 mW/cm^2, which was determined to be sufficient for full cure based on the RT-FTIR reaction kinetics studies.

2. Results and Discussions

3.1 Preparation of TALG and Thiol-Ene Polymer Networks

TALG was synthesized as per our previous report (Fig. 1A) employing NaOH as a mild base in dimethyl sulfoxide.[38] This reaction could be readily performed on large scales (12 g) and the resultant triallyl monomer could be obtained in high yields (80% yield).[38] Although we focused on the triallyl variant for this work, this methodology could be expanded to produce other functional ether and ester derivatives of levoglucosan to modulate the physical and thermo-mechanical properties of crosslinked networks further.

Thiol-ene polymerization of the synthesized TALG monomer was performed with multifunctional, commercially available thiols to produce a family of novel thermoset systems. Four different thiol-crosslinkers comprising of small molecule and polymeric thiols, along with

thiols of varying functionality were investigated (Fig. 1B). Specifically, the four thiol crosslinkers utilized in this work are 1,4-butanediol bis(thioglycolate) (BDBT), trimethylolpropane tris(3-mercaptopropionate) (TPTMP), pentaerythritol tetrakis(3-mercaptopropionate) (PETMP), and ethoxylated trimethylolpropane tris(3-mercaptopropionate) (ETTMP 700). The thiols BDBT, TPTMP, PETMP, and ETTMP 700 are hereby coded as 2SH, 3SH, 4SH and poly3SH, respectively (Fig. 1B). Larsen *et.al.* published a detailed retrosynthetic analysis of the thiols used in the present study, showing that the chosen thiols can be synthesized from renewable resources.[40] This retrosynthetic analysis further supports the overall high bio-based content of the synthesized levoglucosan networks. To systematically investigate the influence of thiol type and thiol:ene stoichiometric ratio on the properties of the resulting polymer networks, 8 different thiol-ene networks were synthesized. The monomer mixture compositions are summarized in Table 1. Omnirad 2100, a commercially available liquid phosphine oxide compound was employed as the photoinitiator for all formulations at a constant mass loading. Ethyl acetate (EA) was selected as a diluent since it is miscible with TALG, Omnirad 2100, and the thiols and thus aides in homogenizing the monomer mixtures. The monomers TALG (η = 13.8 mPa-s), 2SH (13.1 mPa-s), 3SH (150 mPa-s), 4SH (500 mPa-s), and poly3SH (200 mPa-s) are all low-viscosity liquids, which allowed for easier formulation and reduction in the amount of diluent required, and also introduced the potential for solvent-free formulation.[41]

Fig. 1C illustrates network formation *via* thiol-ene photopolymerization of TALG and 4SH monomers. The naming system for the polymer networks prepared is TALG-Thiol Type-Thiol Ratio as shown in Table 1. For instance, TALG-2SH-1 is the network prepared from TALG and 2SH monomers at a thiol:ene ratio of 1:1. The thermoset films prepared using the TALG-2SH-0.5

and TALG-poly3SH-0.5 mixtures were too soft to be tensile tested and will not be discussed further.

Table 1. The formulations of different levoglucosan-based thiol-ene networks. [a]Values in phr: part per hundred of TALG + Thiol mixture.

Sample	Thiol : Ene	TALG (wt%)	2SH (wt%)	3SH (wt%)	4SH (wt%)	poly3 SH (wt%)	Omnirad 2100[a] (phr)	Ethyl acetate[a] (phr)	Gel Fraction (%)
TALG-2SH-0.5	0.5 : 1	61.2	38.8	–	–	–	5	20	-
TALG-3SH-0.5	0.5 : 1	58.6	–	41.4	–	–	5	20	89 ± 9
TALG-4SH-0.5	0.5 : 1	60.6	–	–	39.4	–	5	20	96 ± 4
TALG-poly3SH-0.5	0.5 : 1	44.6	–	–	–	55.4	5	20	-
TALG-2SH-1	1 : 1	44.1	55.9	–	–	–	5	20	93 ± 3
TALG-3SH-1	1 : 1	41.5	–	58.5	–	–	5	20	96 ± 5
TALG-4SH-1	1 : 1	43.5	–	–	56.5	–	5	20	97 ± 1
TALG-poly3SH-1	1 : 1	28.7	–	–	–	71.3	5	20	93 ± 2

3.2 Photopolymerization Kinetics

The detailed curing behaviors and reaction kinetics of the thiol-ene polymer networks were investigated using RT-FTIR spectroscopy. Fig. 2A shows the IR spectra for the TALG-4SH-1 composition before and after UV irradiation. As shown in Fig. 2A, after UV irradiation the

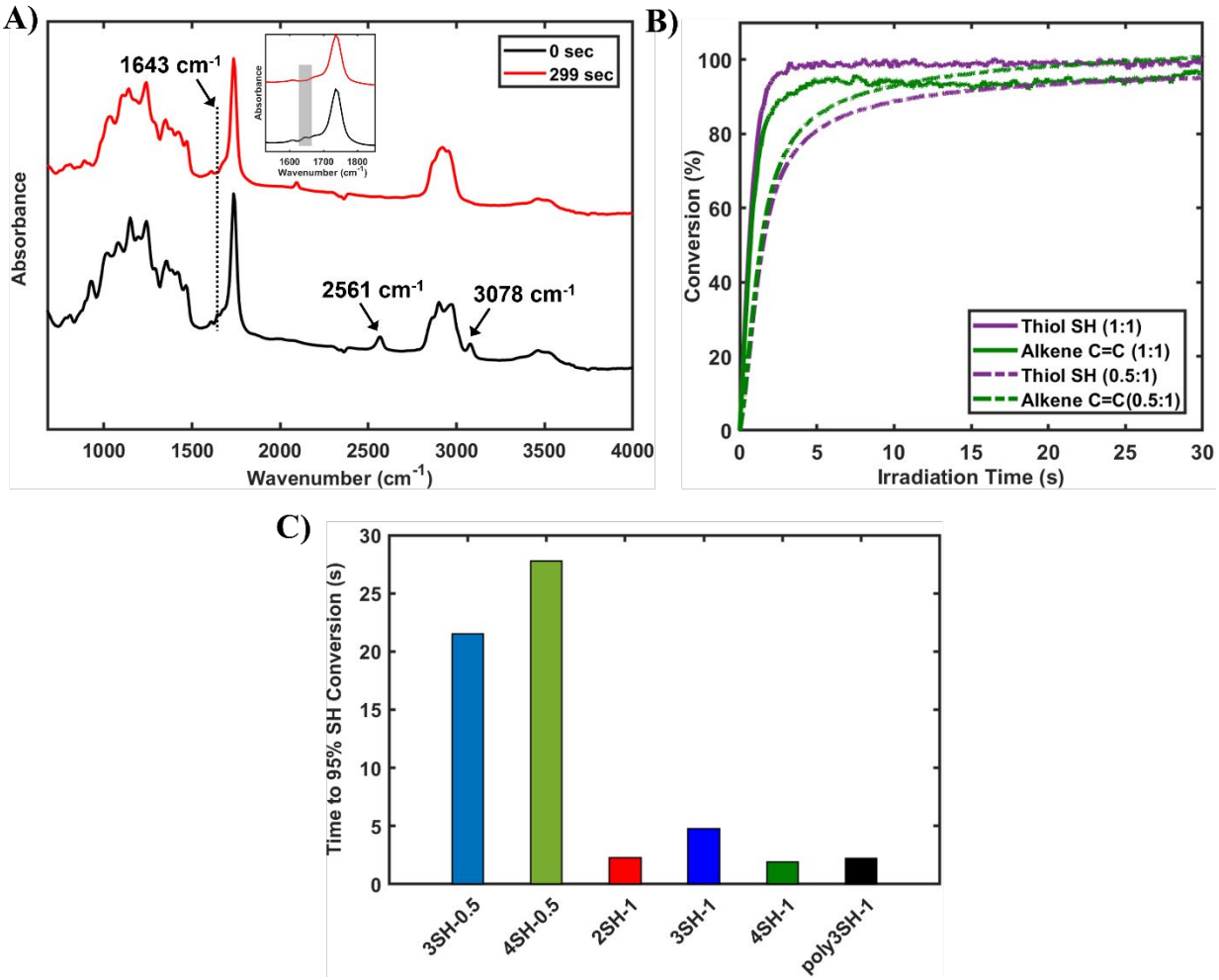

Figure 2 A) FTIR spectra of TALG-4SH-1 at 0 sec (before UV irradiation) and after UV irradiation for 299 sec. B) Conversion of alkene and thiol for TALG-4SH-1 (solid) and TALG 4SH-0.5 (dashed). C) Comparison of thiol reaction kinetics for different levoglucosan-based networks.

absorption peaks corresponding to allyl groups (3078 cm^{-1} and 1643 cm^{-1}) and thiol groups (2561 cm^{-1}) have disappeared, indicating near-full consumption of these two functional groups during the curing process. Furthermore, Fig. 2A shows that the C–H (2780 to 3040 cm^{-1}) and carbonyl

(1680 to 1840 cm^{-1}) absorption peaks are not affected by UV-exposure indicating that the alkyl units and levoglucosan bicyclic rings are preserved. Similar IR spectra for all other compositions are in the Supporting Information (Fig. S1-S5).

The functional group conversion during photopolymerization was calculated based on the peak intensity of the C=C absorption (1643 cm^{-1}) in the allyl groups and the S–H absorption (2561 cm^{-1}) in the thiol groups. Fig. 2B depicts the kinetic data for the TALG-4SH-1 (solid) and TALG 4SH-0.5 (dashed) compositions, respectively. The functional group conversion plots for all other compositions are in the Supporting Information (Fig. S6 – S9). It is immediately evident from Fig. 2B that the TALG-4SH-1 composition approaches maximum conversion much faster than the TALG-4SH-0.5 composition. For instance, the time required for 95% consumption of thiol groups is about 2 s for the TALG-4SH-1 composition, whereas TALG-4SH-0.5 requires about 28 s for 95% thiol consumption (Fig. 2C). This trend is also observed in the TALG-3SH compositions as shown in Fig. 2C. Moreover, as shown in Fig. 2B, it is surprising that for the TALG-4SH-0.5 composition in which the ratio of thiol to ene groups is 0.5:1, the ene conversion approaches a maximum value of >90% instead of an expected ene conversion of close to 50% for a step-growth thiol-ene photopolymerization. This is exhibited by the TALG-3SH-0.5 composition as well (Fig. S6). Finally, the gel fractions of the synthesized thiol-ene networks were measured by extraction with dichloromethane and are shown in Table 1. The gel fraction for all the thermosets ranged between 89 to 97% indicating that levoglucosan-based thiol-ene thermosets are highly crosslinked.

Based on the above observations, it is hypothesized that the allyl groups of TALG undergo other free-radical ene consumption reactions during network synthesis along with the desired thiol-ene reaction, especially in the non-stoichiometric thiol-ene compositions. To assess this hypothesis, a control study was performed by exposing a mixture of TALG, photoinitiator, and

diluent (without the presence of a thiol) to UV light for 15 mins. ^{1}H NMR analysis of the resulting UV-irradiated TALG mixture revealed broadening of peaks and an increase in the integration values (Fig. S10). ^{1}H NMR analysis also revealed no shift in the levoglucosan anomeric proton indicating that no ring-opening of levoglucosan occurred (Fig. S10).[38] Moreover, the viscosity of the TALG mixture also increased after UV irradiation. These observations suggest that the allyl groups of TALG indeed undergo other free-radical ene consumption reactions along with the thiol-ene reaction upon UV exposure. Cramer *et. al.* utilized RT-FTIR spectroscopy to investigate the thiol-ene photopolymerization kinetics for a triallyl-tetrathiol mixture.[42] Their study showed that the conversion of ene functional groups can be as much as 15% greater than the corresponding thiol functional group conversion for the triallyl-tetrathiol system due to the ene's ability to react in the presence of radicals from photoinitiators.[42] To prove this phenomenon, Cramer *et. al.* performed a reaction of the triallyl monomer with the photoinitiator and monitored the reaction *via* RT-FTIR..[42] Their study demonstrated that the triallyl monomer reacted to a substantial extent with ene functional group conversion of up to 25%.[42] Those findings further support our hypothesis that TALG undergoes other free-radical ene consumption reactions during network synthesis. We hypothesize that the allyl groups in TALG potentially participate in both inter- and intra- molecular ene-ene addition reactions, and to some extent degradative chain transfer reactions. Degradative chain transfer has been observed in literature in allyl-containing monomers,[43,44] and is also a possibility for the TALG system. Particularly, the axial orientation and proximity of all the 3 allyl groups in TALG could likely lead to more allylic hydrogen abstraction, yielding allyl radicals that contribute to degradative chain transfer.

The ability of TALG to undergo ene-ene reaction through the allyl groups could be important in applications as biobased reactive diluents for thermosetting resins. Petroleum-based compounds

such as triallyl isocyanurate (TAIC) and styrene are very commonly utilized as reactive diluents in various thermosetting resins such as unsaturated polyesters.[45,46] To obtain biobased thermosets with good performance, it is essential that not only the main resin is bioderived but also the reactive diluents are renewably sourced.[47] Yu *et. al.* reported a series of allylic and vinylic compounds derived from eugenol and vanillin that could be successfully utilized as renewable styrene replacements in dimethacrylated-epoxidized-sucrose-soyate resins.[46] Gallic acid, a bio-based compound, has been used as a renewable TAIC replacement in acrylated epoxidized soybean oil resins upon functionalization with allyl and acryloyl groups.[45] Similarly, TALG exhibits potential as a biobased reactive diluent for thermosetting resins due to its facile one-step synthesis, high allyl functionality, and ability to undergo ene-ene reaction.. Additionally, the reactivity of LG-based diluents can be easily tuned by installing other functional groups such as acrylates.

3.3 Mechanical and Thermal Properties of Thiol-Ene Polymer Networks

Tensile mechanical testing, thermogravimetric analysis (TGA), and differential scanning calorimetry (DSC) were utilized to elucidate the effect of thiol functionality and thiol stoichiometric ratio on the mechanical and thermal properties of levoglucosan-based thermosets. The typical stress-strain curve for each thiol-ene network is depicted in Fig. 3A. The tensile strength, elongation at break, and Young's modulus were calculated from these stress-strain curves and the corresponding results are summarized in Table 2. The mechanical performance of the obtained levoglucosan-based thiol-ene networks could be tailored by controlling the functionality and stoichiometric ratio of thiol crosslinker. The elongation at break of levoglucosan-based thermosets ranges from 19% to 35% indicating that these materials have moderate flexibility. The Young's modulus of levoglucosan-based thermosets can be tuned over a wide range of 3.3 MPa to 14.5 MPa. As shown in Fig. 3A and Table 2, the networks with a 1:1 thiol:ene ratio had a higher

tensile strength and a much higher Young's modulus than the networks with 0.5:1 thiol:ene ratio. While comparing networks with the same thiol:ene ratio and different thiol functionality, the tensile strength and Young's modulus follows the general trend of 2SH < poly3SH < 3SH < 4SH in accordance with other thiol-ene networks reported in the literature (Fig. 3A and Table 2).[40,48] Overall, the mechanical properties of levoglucosan-based thermosets are on par and in some cases

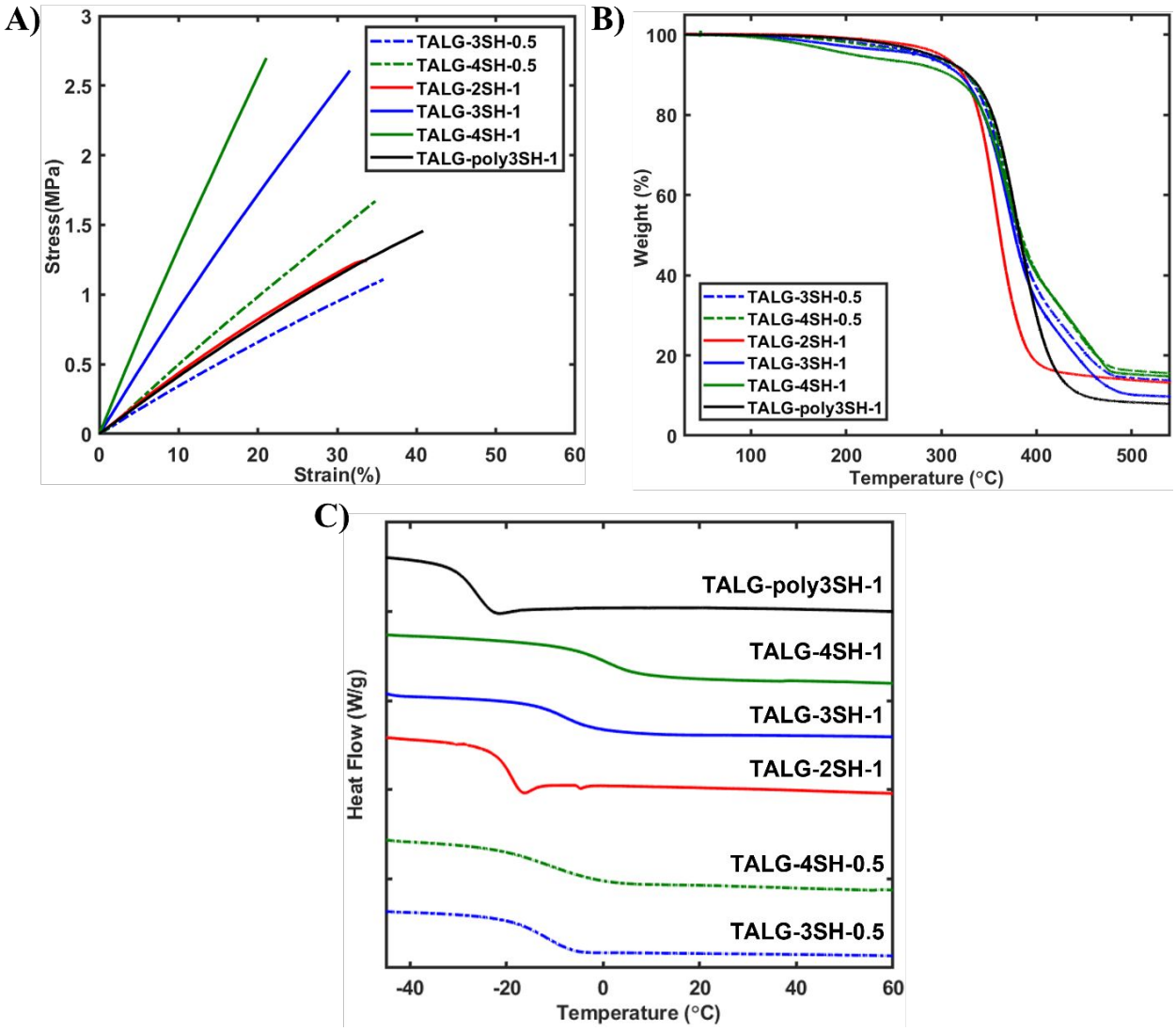

superior to other bioderived thiol-ene networks reported in literature, likely owing to the high allyl functionality and rigid bicyclic structure of levoglucosan.[8,40,49] For example, Larsen *et. al.* synthesized a series of thiol-ene networks from the biobased molecule 2,5-furandicarboxylic acid, resulting in crosslinked networks with Young's modulus ranging from 0.67 MPa to 4.8 MPa.[40]

Similarly, Dai *et. al.* developed a library of thiol-ene networks from eugenol and itaconic acid with Young's modulus in the range of 6.9 MPa to 16.9 MPa.[8]

Figure 3 A) Tensile stress-strain curves of 0.5:1 thiol:ene networks (dashed lines) and 1:1 thiol:ene networks (solid lines). B) TGA curves of curves of 0.5:1 thiol:ene networks (dashed lines) and 1:1 thiol:ene networks (solid lines). C) DSC curves of curves of 0.5:1 thiol:ene networks (dashed lines) and 1:1 thiol:ene networks (solid lines).

Table 2 Mechanical properties of levoglucosan-based networks.

Sample	Tensile Strength (MPa)	Elongation at break (%)	Young's Modulus (MPa)
TALG-3SH-0.5	1.1 ± 0.02	35.2 ± 2.3	3.34 ± 0.07
TALG-4SH-0.5	1.42 ± 0.26	28.3 ± 4.6	4.17 ± 0.84
TALG-2SH-1	1.07 ± 0.14	29.8 ± 3.8	4.14 ± 0.23
TALG-3SH-1	2.06 ± 0.38	24.4 ± 5.1	8.92 ± 0.12
TALG-4SH-1	2.73 ± 0.67	19.9 ± 5.1	14.49 ± 0.58
TALG-poly3SH-1	1.37 ± 0.14	32.3 ± 7.6	4.66 ± 0.81

The thermal stability of the obtained thiol-ene networks was analyzed *via* TGA. Figure 3B presents the TGA curves for all thiol-ene networks and the associated data is summarized in Table 3. The thermal decomposition profile of networks comprising of 2SH and poly3SH was single step, whereas networks prepared from 3SH and 4SH showed a more complex multi-step degradation profile. This observation coincides with previous results of thiol-ene networks synthesized from 3SH, 4SH, and renewably-derived allylic compounds, and is likely due to the presence of ester groups that can break by pyrolytic β-elimination processes.[15,40,50] In general, levoglucosan-based thiol-ene networks possess excellent thermal stability with a $T_{d,10\%}$ (10% mass loss temperature) of >305 ℃ for all networks (Table 3). Interestingly, thiol functionality and thiol stoichiometric ratio did not significantly influence the thermal stability of thiol-ene networks

(Table 3). Furthermore, the char yield of levoglucosan-based networks ranged between 7.9 to 15.5%, which is similar to other eugenol-based thiol-ene networks, possibly due to the bicyclic nature of TALG.[11,17] Lastly, for all the thiol-ene networks no mass loss was observed around 77 ℃ (boiling point of EA), indicating that there was no residual EA entrapped in the networks.

The glass transition temperature (T_g) of all the thermoset materials was determined by DSC as the midpoint of the transition, and the DSC thermograms shown in Fig. 3C. Firstly, no exothermic or endothermic peaks were observed in the thermograms indicating that levoglucosan-based thermosets are amorphous. The T_g values calculated from the DSC thermograms are reported in Table 3 show that the T_g of levoglucosan-based thermosets lies below room temperature. TALG-2SH-1 and TALG-poly3SH-1 have the lowest T_g's of –20.8 ℃ and –26.9 ℃ respectively. As we move towards systems with higher thiol functionality, namely TALG-3SH-1 and TALG-4SH-1, the T_g increases drastically to –6.6 ℃ and 1.2 ℃, respectively. In addition, decreasing the thiol:ene ratio to 0.5:1 from 1:1 causes the T_g of thiol-ene networks to decrease. TALG-3SH-0.5 and TALG-4SH-0.5 have a T_g of –12.1 ℃ and –8 ℃ respectively, as opposed to –6.6 ℃ for TALG-3SH-1 and 1.2 ℃ for TALG-4SH-1. Altogether these results exemplify that the thermal properties of levoglucosan-derived thiol-ene networks can be tailored by modifying the thiol functionality and the thiol stoichiometric ratio. Similarly, the physical and thermomechanical properties can also be modulated by using other functional derivatives of levoglucosan.

3.4 Viscoelastic Properties of Thiol-Ene Polymer Networks The viscoelastic behavior of thiol-ene networks as a function of temperature was investigated using dynamic mechanical analysis (DMA) with a tensile clamp geometry. The storage modulus (E') and dissipation factor (tan δ) data for the networks with thiol:ene ratio of 1:1 are shown in Fig. 4A and 4B respectively. The corresponding data for the networks with thiol:ene ratio of 0.5:1 is shown in Fig. S11. As shown

in Fig. 4A, all thiol-ene networks exhibit a similar trend of storage modulus as a function of temperature. Initially, all the thiol-ene networks are in the glassy state with a E' value of the order of 1000 MPa. As the temperature increases, the relaxation processes within the network become more significant and E' gradually decreases. Upon further increasing the temperature, the polymer networks reach a rubbery state leading to a plateau in the storage modulus. Table 3 shows the rubbery plateau modulus for all thiol-ene networks, and the results indicate that the stiffness of levoglucosan-based thermosets can be tuned over the wide range of 2.53 MPa to 19.42 MPa by varying the thiol functionality and stoichiometric ratio.

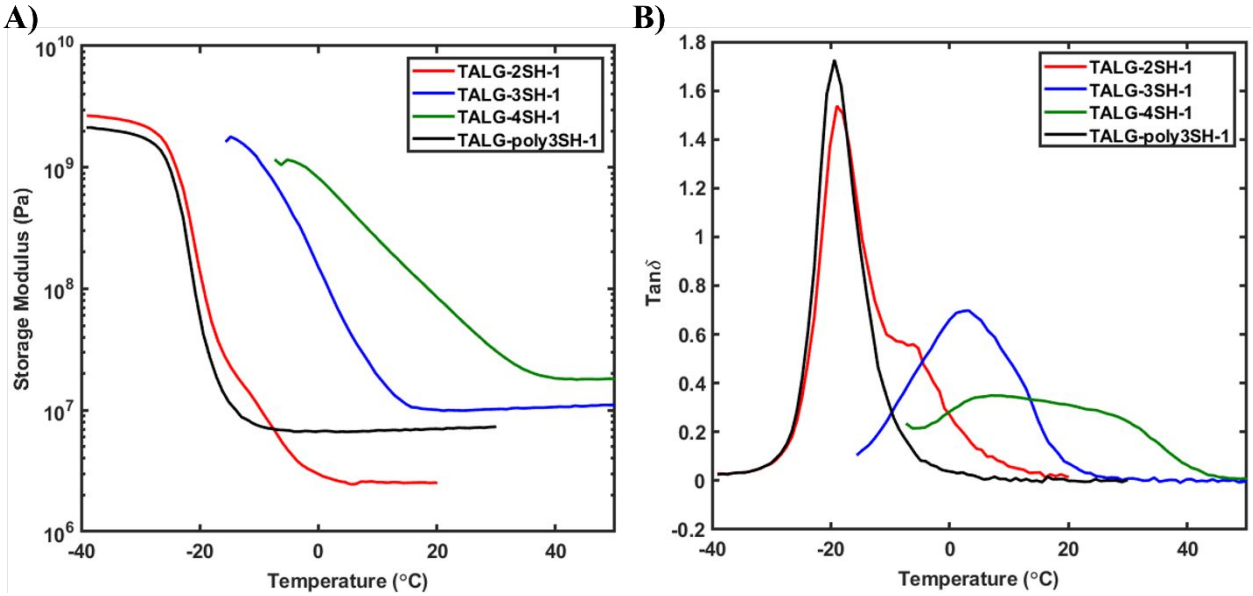

Figure 4 DMA curves depicting A) storage modulus and B) tan δ for 1:1 thiol:ene networks.

The rubbery plateau modulus was also used to calculate the average molecular weight between crosslinking points (M_c) and the crosslink density (v) using eqns. 2 and 3 derived from the statistical mechanical theory of rubbery elasticity.[51] In these equations, ρ is the density of the thermoset, T is the absolute temperature, and R is the universal gas constant. The results are summarized in Table 3. Comparing the different networks, the crosslink densities ranged as follows: TALG-4SH-1 > TALG-3SH-1 > TALG-poly3SH-1 > TALG-4SH-0.5 > TALG-3SH-0.5 > TALG-2SH-1. It should be noted that the cross-link density values are used only for qualitative

comparison since eqns. 2 and 3 cannot accurately predict *v* for highly cross-linked thermosets.[51] At a constant thiol:ene ratio, the crosslink density increases with thiol functionality since the number of reactive sites increases and similarly, at a constant thiol functionality, the crosslink density increases with increasing thiol content. Moreover, the results of DMA analysis corroborate very well with the trends observed from tensile testing and DSC as reported in section 3.3.

$$M_c = \frac{3\rho RT}{E'} \quad (2)$$

$$\nu = \frac{\rho}{M_C} \quad (3)$$

Table 3 The thermomechanical and thermal stability properties of levoglucosan based networks

Sample	T_g DSC (℃)	T_g DMA (℃)	Rubbery Modulus (MPa, Tg + 30℃)	M_c (g/mol)	$\nu \times 10^{-3}$ (mol/cm^3)	$T_{d,10\%}$ (℃)	Char yield (%)
TALG-3SH-0.5	–12.1	–10.6	3.44	2480	0.48	327.6	13.7
TALG-4SH-0.5	–8	–7.1	4.59	2060	0.63	326.7	15.5
TALG-2SH-1	–20.8	–19	2.53	2190	0.37	323.4	13.1
TALG-3SH-1	–6.6	3.2	10.45	880	1.37	319	9.7
TALG-4SH-1	1.2	6.9	19.42	470	2.51	307.6	14.7
TALG-poly3SH-1	–26.9	–19.4	6.85	1250	0.97	329	7.9

Lastly, DMA can also be utilized to determine the T_g of a crosslinked network by recording the temperature corresponding to the maximum peak in the tan δ curves (Table 3). As shown in Fig. 4B and Fig. S11, almost all thiol-ene networks show one tan δ peak except for TALG-2SH-1 which shows a second smaller tan δ peak along with the predominant maximum peak. This implies existence of some heterogeneity in TALG-2SH-1, potentially more network defects such as dangling ends and loops due to the lower thiol functionality. Table 3 also shows that the T_g values calculated by DMA agree well with the T_g values determined *via* DSC.

3.5 Degradation Behavior of Thiol-Ene Polymer Networks

The hydrolytic degradability of levoglucosan-based thermosets was investigated based on the

inherent ester linkages in the thiol-ene networks which are well-known to be susceptible to base-

mediated hydrolysis. For this study, the degradability of only the thiol-ene networks with the thiol:ene ratio of 1:1 was evaluated. The effect of both base strength and presence of organic solvent on the thermoset degradation profile was studied. To understand the effect of base strength, degradation studies were conducted in 0.1 M, 0.5 M, and 1 M NaOH at room temperature. It has been reported that the addition of a good solvent in the degradation solution promotes swelling and wettability of the thermoset sample and enhances the solubility of degradation products thereby leading to faster degradation.[52–54] Hence, degradation studies were also performed by immersing the thermosets in 0.1 M NaOH/THF (water/THF (v/v) = 1:1) and 0.1 M NaOH/Acetone (water/acetone (v/v) = 1:1) solutions at room temperature. As a control, the swelling ratio of TALG-poly3SH-1 was determined and it was found to be 16.7% in water, 113% in THF, and 52.5% in acetone indicating that the presence of THF will likely promote faster degradation due

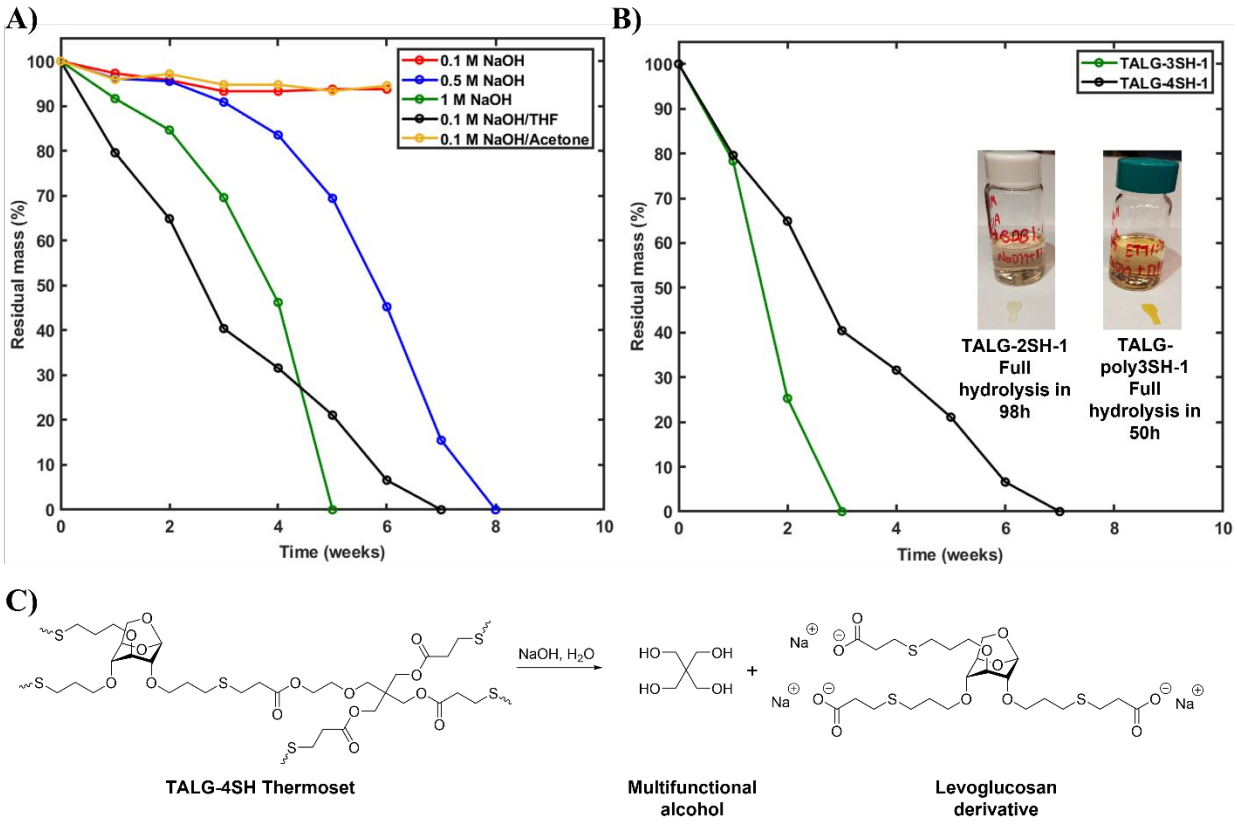

to easier penetration of solvent and base molecules in the network.**Figure 5** A) Mass loss of

TALG-4SH-1 under different degradation conditions. B) Mass loss of different thermoset samples in 0.1 M NaOH/THF. C) Degradation of levoglucosan-based thermosets into alcohol and carboxylic byproducts.

Fig. 5A depicts the mass loss of TALG-4SH-1 thermosets under different degradation conditions. As shown in Fig. 5A, thermoset degradation rate increases dramatically with a slight increase in base strength. In a 0.1 M NaOH solution, TALG-4SH-1 networks undergo just 6% mass loss in 6 weeks, whereas the network is completely degraded into soluble molecules in about 8 weeks when immersed in 0.5 M NaOH, and in about 5 weeks when immersed in 1 M NaOH. Similarly, the type of organic solvent employed also had a drastic effect on the degradation profile. Interestingly, the addition of acetone to 0.1 M NaOH had a negligible effect on degradation rate, as shown in Fig. 5A. On the other hand, the incorporation of THF in the degradation solution promoted faster degradation (in line with the control swelling test) such that the thermoset completely disappeared in 7 weeks. Since THF can be prepared from biomass sources, this method of accelerating hydrolysis using THF based solutions could be useful as a sustainable end-of-life pathway. It should be noted that under all the different degradation conditions, the materials were observed to degrade *via* a surface erosion mechanism, exhibiting a gradual loss in size.

Fig. 5B compares the mass loss of different thermoset samples when immersed in 0.1 M NaOH/THF solution. In the presence of THF, the networks TALG-poly3SH-1 and TALG-2SH-1 undergo rapid and complete hydrolysis in ~50 h and ~98 h respectively (insets in Fig. 5B). Furthermore, TALG-3SH-1 is completely degraded in 3 weeks and TALG-4SH-1 is completely hydrolyzed in 7 weeks under the same conditions. Hence, the degradation time in the presence of THF varies as follows: TALG-poly3SH-1 < TALG-2SH-1 < TALG-3SH-1 < TALG-4SH-1. This difference in degradation time can be explained based on the hydrophobicity of thiol and the

crosslink density of networks. TALG-3SH-1 and TALG-4SH-1 have the highest crosslink densities and T_g and therefore are the slowest to degrade. Although TALG-poly3SH-1 has a higher crosslink density than TALG-2SH-1, the polyethylene glycol units in the structure of poly3SH likely enhance the hydrophilicity of TALG-poly3SH-1 networks thus promoting faster degradation.

The solubilized degradation products of the basic degradation conditions were characterized for all networks *via* ^{1}H NMR analysis. The visualization image of the degradation products of TALG-4SH-1 is shown in Fig. 5C. As a result of the hydrolysis, a multifunctional alcohol and a levoglucosan based tricarboxylic acid with a sulfide bond were collected as main degradation products for all networks (Fig. S12 – S15). These results suggest that levoglucosan-based thermosets can completely degrade into small soluble molecules leaving behind no microplastic fragments. Although the degradation products are different from the starting materials, it is worth noting that the multifunctional alcohol formed *via* hydrolysis can be recovered and then refunctionalized to synthesize multifunctional thiols or other polymerizable groups, thus allowing these molecules to be re-introduced as a feedstock into the application space. Additionally, the levoglucosan based tricarboxylic acid could potentially be utilized as a multifunctional carboxylic acid for the synthesis of biobased polyester resins or as a crosslinker for biobased epoxy resins. Further, the levoglucosan based tricarboxylic acid could possibly be digested by levoglucosan kinase (an enzyme that assimilates levoglucosan) or by other levoglucosan-metabolizing bacteria reported in literature,[55,56] however further study would be needed to prove this. Overall, these thiol–ene networks can serve as reliable structural materials during their lifetime and degrade under ambient conditions after use.

3.6 3D Printing

One immediate application for TALG is in resins for additive manufacturing or 3D printing. The vast majority of current commercial feedstocks for photopolymerizable resins in various additive manufacturing techniques such as SLA or DIW are petroleum-derived. We suggest that TALG-based resins are excellent candidates for more sustainable rapid prototyping *via* 3D printing, as they offer the dual advantage of being renewably sourced and having a clear end-of-life pathway through hydrolysis-based degradation, instead of landfilling or environmental contamination.

To illustrate that the TALG thiol-ene resins could be potentially utilized to create a sustainable rapid prototyping process via 3D printing, we sought to develop a printable TALG-based resin and demonstrate its degradation for more sustainable end-of-life. We selected the TALG-poly3SH-1 resin for 3D printing demonstration due to its rapid degradation kinetics and intermediate mechanical properties. We chose UV-assisted DIW printing process as outlined in the schematic in Fig. 6A to print parts,[57,58] and with an image of the printing process in Fig. 6B. Similar to previous work, hydrophilic fumed silica (12-14 wt.%) was added to the TALG-poly3SH-1 resin as a rheology modifier to provide a sufficient yield stress to ensure quality printing.[59,60] By adding the fumed silica particles, the TALG-poly3SH-1 resin was transformed from a low viscosity Newtonian fluid into a shear thinning paste (Fig. S16) with high viscosity in the low shear rate regime (>1000 Pa s). Oscillatory rheology measurements (Fig. S17) demonstrated that the printing resin with silica demonstrated solid-like behavior (storage modulus ~ 1000 Pa) at low shear stresses and at elevated shear stress displayed yielding (σ_{yield} ~ 500 Pa). Both of these measurements indicated the suitability of the resin for DIW printing as it prevents distortion of the deposited material between leaving the nozzle and curing. During printing, after a layer was completed, the part was exposed to a UV light with an intensity of 25 mW/cm^2 for 10s to ensure

curing of the part (see Supplemental Video). Printed parts show excellent print fidelity as compared to digital files, as shown in Fig. 6C.

Finally, we were interested in studying the hydrolysis of the 3D printed parts and investigating the effects of rheology modifying additives such as silica on the degradation behavior. The hydrolysis of the 3D printed leaves was studied by immersing the leaves in 10 ml of 1 M NaOH, 1 M HCl, de-ionized water, and artificial seawater at room temperature with no agitation. Degradation was indicated by clear visible dissolution of the printed leaf. Fig. 6D depicts the hydrolysis in 1 M NaOH solution, and shows that after 3 hours of immersion the degradation solution slowly starts turning yellow. Over the course of 9 hours, the leaf thickness decreases remarkably, and the porous features of the leaf visibly become larger. Ultimately, in about 30 hours the printed leaf had completely dissolved leaving behind a yellow NaOH solution. As shown in Fig. 6D, the hydrophilic fumed silica used as rheology modifier remains intact in the degradation solution. The remaining hydrophilic fumed silica was recovered in quantitative amounts and can likely be reused for the next printing cycle. Fig. 6D also depicts a surface erosion hydrolysis mechanism with a gradual decrease in leaf size, consistent with the thermoset film degradation studies. Remarkably, no degradation of the 3D printed leaves was observed over the course of 8 weeks when immersed in 1 M HCl, de-ionized water, and artificial seawater at room temperature. These results indicate that levoglucosan-based 3D printed parts can undergo triggered degradation under basic conditions, and these networks are highly stable in acidic and aqueous environments. Overall, these results are very promising and signify that levoglucosan-based printed parts have a clear end-of-life pathway *via* base-triggered hydrolytic degradation, and this property will help mitigate 3D printed plastic waste. Furthermore, these levoglucosan-based thiol-ene resins can also be easily utilized in other 3D printing processes upon proper formulation.

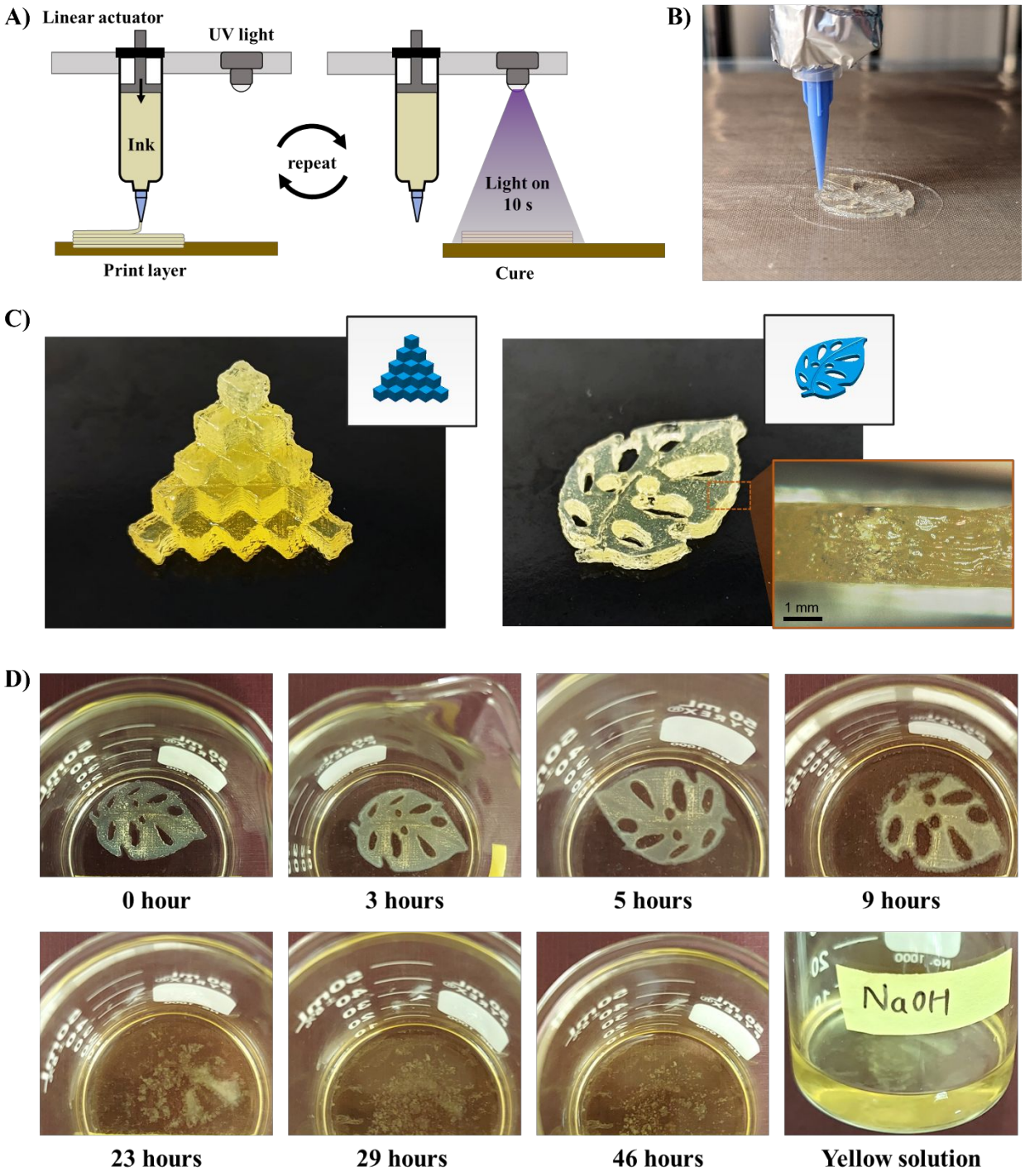

Figure 6 A) Schematic depicting the Direct Ink-Writing (DIW) 3D printing process. B) A picture of the printing process with TALG-poly3SH-1. C) 3D printed parts from TALG-poly3SH-1. D) Hydrolytic degradation of 3D printed leaf in 1 M NaOH solution.

3. Conclusions

In this work, we have synthesized a family of scalable triallyl levoglucosan based networks through UV-initiated thiol-ene chemistry using four different commercially-available multifunctional thiols. Both the levoglucosan precursor and the multifunctional thiols can be renewably sourced, leading to overall high bio-based content of the synthesized networks. Through real-time Fourier-transform infrared spectroscopy the thiol-ene photopolymerization kinetics were investigated in-depth for each network. The RT-FTIR studies revealed that the allyl groups of TALG undergo free-radical homopolymerization upon UV-exposure, and this property could be important for application of TALG as biobased reactive diluent for thermosetting resins. The levoglucosan-based thermosets showed tunable thermomechanical properties and hydrolytic degradation rates based on the type and stoichiometric ratio of thiol crosslinker employed. The Young's modulus and glass transition temperature of levoglucosan-based networks could be tuned over the wide range of 3.3 MPa to 14.5 MPa and –19.4 ℃ to 6.9 ℃, respectively. To demonstrate the suitability of levoglucosan-based thiol-ene resins for extrusion-based 3D printing, the TALG-poly3SH-1 resin was 3D printed via UV-assisted DIW to create intricate 3D printed parts with excellent print fidelity. Finally, the hydrolytic degradability of the 3D printed objects was demonstrated, whereby the 3D printed leaf hydrolyzed completely into small soluble molecules within 30 hours when immersed in an aqueous NaOH solution. These results demonstrate that TALG-based resins are excellent candidates for sustainable rapid prototyping as they offer the dual advantage of being renewably sourced and having a clear end-of-life pathway through hydrolysis. Overall, levoglucosan exhibits great potential as a renewable platform chemical for the development of tailored thermosets that could be important in applications ranging from 3D printing to biomaterials.

Author Contributions

M.K.P. wrote the manuscript and performed all the bulk thermoset film experimental studies and data analysis. M.M.H. performed all the 3D printing and viscosity experimental studies and wrote the related text and figures in the manuscript. C.J.E. and T.M.R. provided mentorship, research direction, and edited the manuscript.

Conflicts of interest

There are no conflicts to declare.

Acknowledgements

This work was supported and funded by the NSF Center for Sustainable Polymers at the University of Minnesota; a National Science Foundation supported Center for Chemical Innovation (CHE-1901635). The authors acknowledge John Beumer for preparing the TOC graphic.

References

1 S. Ma and D. C. Webster, Degradable thermosets based on labile bonds or linkages: A review, *Prog. Polym. Sci.*, 2018, **76**, 65–110.

2 W. Post, A. Susa, R. Blaauw, K. Molenveld and R. J. I. Knoop, A Review on the Potential and Limitations of Recyclable Thermosets for Structural Applications, *Polym. Rev.*, 2020, **60**, 359–388.

3 R. A. Ortiz, A. E. Garcia Valdéz, M. G. Martinez Aguilar and M. L. Berlanga Duarte, An effective method to prepare sucrose polymers by Thiol-Ene photopolymerization, *Carbohydr. Polym.*, 2009, **78**, 282–286.

4 Q. Zhang, H. R. Phillips, A. Purchel, J. K. Hexum and T. M. Reineke, Sustainable and Degradable Epoxy Resins from Trehalose, Cyclodextrin, and Soybean Oil Yield Tunable Mechanical Performance and Cell Adhesion, *ACS Sustain. Chem. Eng.*, 2018, **6**, 14967–

14978.

5 J. J. Gallagher, M. A. Hillmyer and T. M. Reineke, Degradable thermosets from sugar-derived dilactones, *Macromolecules*, 2014, **47**, 498–505.

6 S.-S. Kim, C. M. Lau, L. M. Lillie, W. B. Tolman, T. M. Reineke and C. J. Ellison, Degradable Thermoset Fibers from Carbohydrate-Derived Diols via Thiol–Ene Photopolymerization, *ACS Appl. Polym. Mater.*, 2019, **1**, 2933–2942.

7 K. T. Wacker, A. C. Weems, S. M. Lim, S. Khan, S. E. Felder, A. P. Dove and K. L. Wooley, Harnessing the Chemical Diversity of the Natural Product Magnolol for the Synthesis of Renewable, Degradable Neolignan Thermosets with Tunable Thermomechanical Characteristics and Antioxidant Activity, *Biomacromolecules*, 2019, **20**, 109–117.

8 J. Dai, S. Ma, L. Zhu, S. Wang, L. Yang, Z. Song, X. Liu and J. Zhu, UV-thermal dual cured anti-bacterial thiol-ene networks with superior performance from renewable resources, *Polymer (Guildf).*, 2017, **108**, 215–222.

9 J. T. Trotta, A. Watts, A. R. Wong, A. M. Lapointe, M. A. Hillmyer and B. P. Fors, Renewable Thermosets and Thermoplastics from Itaconic Acid, *ACS Sustain. Chem. Eng.*, 2019, **7**, 2691–2701.

10 H. Sajjad, L. M. Lillie, C. M. Lau, C. J. Ellison, W. B. Tolman and T. M. Reineke, Degradable polyanhydride networks derived from itaconic acid, *Polym. Chem.*, 2021, **12**, 608–617.

11 Y. Tian, Q. Wang, J. Cheng and J. Zhang, A fully biomass based monomer from itaconic acid and eugenol to build degradable thermosets: Via thiol-ene click chemistry, *Green Chem.*, 2020, **22**, 921–932.

12 T. Yoshimura, T. Shimasaki, N. Teramoto and M. Shibata, Bio-based polymer networks by thiol-ene photopolymerizations of allyl-etherified eugenol derivatives, *Eur. Polym. J.*, 2015, **67**, 397–408.

13 J. T. Miao, L. Yuan, Q. Guan, G. Liang and A. Gu, Water-Phase Synthesis of a Biobased Allyl Compound for Building UV-Curable Flexible Thiol-Ene Polymer Networks with High Mechanical Strength and Transparency, *ACS Sustain. Chem. Eng.*, 2018, **6**, 7902–7909.

14 T. Liu, L. Sun, R. Ou, Q. Fan, L. Li, C. Guo, Z. Liu and Q. Wang, Flame retardant eugenol-based thiol-ene polymer networks with high mechanical strength and transparency, *Chem. Eng. J.*, 2019, **368**, 359–368.

15 D. Guzmán, A. Serra, X. Ramis, X. Fernández-Francos and S. De la Flor, Fully renewable thermosets based on bis-eugenol prepared by thiol-click chemistry, *React. Funct. Polym.*, 2019, **136**, 153–166.

16 J. Xue, X. Yang, Y. Ke, Z. Yan, X. Dong, Y. Luo and C. Zhang, Novel eugenol-based allyl-terminated precursors and their bio-based polymer networks through thiol-ene click reaction, *Ind. Crops Prod.*, 2021, **171**, 113956.

17 Z. Lin, Y. Ke, X. Peng, X. Wu, C. Zhang, H. Zhao and P. Feng, Thermally Stable , Solvent Resistant , and Multifunctional Thermosetting Polymer Networks with High Mechanical Properties Prepared from Renewable Plant Phenols via Thiol − Ene Photo Click Chemistry, *ACS Appl. Polym. Mater.*, 2022, **4**, 5330–5340.

18 C. E. Hoyle and C. N. Bowman, Thiol-ene click chemistry, *Angew. Chemie - Int. Ed.*, 2010, **49**, 1540–1573.

19 E. M. Maines, M. K. Porwal, C. J. Ellison and T. M. Reineke, Sustainable advances in

SLA/DLP 3D printing materials and processes, *Green Chem.*, 2021, **23**, 6863–6897.

20 X. Kuang, D. J. Roach, J. Wu, C. M. Hamel, Z. Ding, T. Wang, M. L. Dunn and H. J. Qi, Advances in 4D Printing: Materials and Applications, *Adv. Funct. Mater.*, 2019, **29**, 1–23.

21 R. Ding, Y. Du, R. B. Goncalves, L. F. Francis and T. M. Reineke, Sustainable near UV-curable acrylates based on natural phenolics for stereolithography 3D printing, *Polym. Chem.*, 2019, **10**, 1067–1077.

22 J. T. Miao, S. Peng, M. Ge, Y. Li, J. Zhong, Z. Weng, L. Wu and L. Zheng, Three-Dimensional Printing Fully Biobased Heat-Resistant Photoactive Acrylates from Aliphatic Biomass, *ACS Sustain. Chem. Eng.*, 2020, **8**, 9415–9424.

23 S. Grauzeliene, M. Kastanauskas, V. Talacka and J. Ostrauskaite, Photocurable Glycerol- and Vanillin-Based Resins for the Synthesis of Vitrimers, *ACS Appl. Polym. Mater.*, 2022, **4**, 6103−6110.

24 S. G. Sabine Briede, Maksims Jurinovs, Sergey Nechausov, Oskars Platnieks, State-of-the-art UV-assisted 3D printing via a rapid syringe-extrusion approach for photoactive vegetable oil acrylates produced in one-step synthesis, *Mol. Syst. Des. Eng.,* 2022, **7**, 1434-144825 D. G. Sycks, T. Wu, H. S. Park and K. Gall, Tough, stable spiroacetal thiol-ene resin for 3D printing, *J. Appl. Polym. Sci.*, 2018, **135**, 1–12.

26 C. C. Cook, E. J. Fong, J. J. Schwartz, D. H. Porcincula, A. C. Kaczmarek, J. S. Oakdale, B. D. Moran, K. M. Champley, C. M. Rackson, A. Muralidharan, R. R. McLeod and M. Shusteff, Highly Tunable Thiol-Ene Photoresins for Volumetric Additive Manufacturing, *Adv. Mater.*, 2020, **32**, 1–6.

27 Y. Wu, M. C. Simpson and J. Jin, Fast Hydrolytically Degradable 3D Printed Object Based on Aliphatic Polycarbonate Thiol-Yne Photoresins, *Macromol. Chem. Phys.*, 2021,

222, 1–7.

28 D. Merckle, E. Constant and A. C. Weems, Linalool Derivatives for Natural Product-Based 4D Printing Resins, *ACS Sustain. Chem. Eng.*, 2021, **9**, 36, 12213–12222.

29 E. Constant, O. King and A. C. Weems, Bioderived 4D Printable Terpene Photopolymers from Limonene and β-Myrcene, *Biomacromolecules*, 2022, **23**, 6, 2342–2352..

30 L. Li, Q. Lin, M. Tang, A. J. E. Duncan and C. Ke, Advanced Polymer Designs for Direct-Ink-Write 3D Printing, *Chem. - A Eur. J.*, 2019, **25**, 10768–10781.

31 J. A. Lewis, Direct ink writing of 3D functional materials, *Adv. Funct. Mater.*, 2006, **16**, 2193–2204.

32 A. Medellin, W. Du, G. Miao, J. Zou, Z. Pei and C. Ma, Vat photopolymerization 3d printing of nanocomposites: A literature review, *J. Micro Nano-Manufacturing*, 2019, **7**, 3, 031006 - 031017

33 M. Zheng, Q. Guo, X. Yin, N. N. Getangama, J. R. de Bruyn, J. Xiao, Y. Bai, M. Liu and J. Yang, Direct ink writing of recyclable andin siturepairable photothermal polyurethane for sustainable 3D printing development, *J. Mater. Chem. A*, 2021, **9**, 6981–6992.

34 M. A. Skylar-Scott, J. Mueller, C. W. Visser and J. A. Lewis, Voxelated soft matter via multimaterial multinozzle 3D printing, *Nature*, 2019, **575**, 330–335.

35 S. Maduskar, V. Maliekkal, M. Neurock and P. J. Dauenhauer, On the Yield of Levoglucosan from Cellulose Pyrolysis, *ACS Sustain. Chem. Eng.*, 2018, **6**, 7017–7025.

36 M. R. Rover, A. Aui, M. M. Wright, R. G. Smith and R. C. Brown, Production and purification of crystallized levoglucosan from pyrolysis of lignocellulosic biomass, *Green Chem.*, 2019, **21**, 5980–5989.

37 J. Wang, Z. Lu and A. Shah, Techno-economic analysis of levoglucosan production via

fast pyrolysis of cotton straw in China, *Biofuels, Bioprod. Biorefining*, 2019, **13**, 1085–1097.

38 M. K. Porwal, Y. Reddi, D. J. Saxon, C. J. Cramer, C. J. Ellison and T. M. Reineke, Stereoregular functionalized polysaccharides via cationic ring-opening polymerization of biomass-derived levoglucosan , *Chem. Sci.*, 2022, **13**, 4512–4522.

39 P. R. De Souza Mendes, A. A. Alicke and R. L. Thompson, Parallel-plate geometry correction for transient rheometric experiments, *Appl. Rheol.*, 2014, **24**, 1–10.

40 D. B. Larsen, R. Sønderbæk-Jørgensen, J. Duus and A. E. Daugaard, Investigation of curing rates of bio-based thiol-ene films from diallyl 2,5-furandicaboxylate, *Eur. Polym. J.*, 2018, **102**, 1–8.

41 A. Badria, D. J. Hutchinson, N. Sanz del Olmo and M. Malkoch, Acrylate-free tough 3D printable thiol-ene thermosets and composites for biomedical applications, *J. Appl. Polym. Sci.*, 2022, **139**, 1–10.

42 N. B. Cramer and C. N. Bowman, Kinetics of thiol-ene and thiol-acrylate photopolymerizations with real-time Fourier transform infrared, *J. Polym. Sci. Part A Polym. Chem.*, 2001, **39**, 3311–3319.

43 S. J. Oh, D. R. Kinney, W. Wang and P. L. Rinaldi, Studies of allyl alcohol radical polymerization by PFG-HMQC and HMBC NMR at 750 MHz, *Macromolecules*, 2002, **35**, 2602–2607.

44 P. Chen, Y. Zhou, Q. Li, Q. Xiao, Y. Lun, Y. Huang and G. Ye, Study on the photopolymerization mechanism of allyl monomers: A photo-driven radical-mediated [3+2] cyclopolymerization mechanism to reduce degradation chain transfer, *Polymer (Guildf).*, 2022, **255**, 125153.

45 S. Ma, Y. Jiang, X. Liu, L. Fan and J. Zhu, Bio-based tetrafunctional crosslink agent from gallic acid and its enhanced soybean oil-based UV-cured coatings with high performance, *RSC Adv.*, 2014, **4**, 23036–23042.

46 A. Z. Yu, E. M. Serum, A. C. Renner, J. M. Sahouani, M. P. Sibi and D. C. Webster, Renewable Reactive Diluents as Practical Styrene Replacements in Biobased Vinyl Ester Thermosets, *ACS Sustain. Chem. Eng.*, 2018, **6**, 12586–12592.

47 J. Liu, S. Wang, Y. Peng, J. Zhu, W. Zhao and X. Liu, Advances in sustainable thermosetting resins: From renewable feedstock to high performance and recyclability, *Prog. Polym. Sci.*, 2021, **113**, 101353.

48 Z. Lin, Y. Ke, X. Peng, X. Wu, C. Zhang, H. Zhao and P. Feng, Thermally Stable , Solvent Resistant , and Multifunctional Thermosetting Polymer Networks with High Mechanical Properties Prepared from Renewable Plant Phenols via Thiol − Ene Photo Click Chemistry, *ACS Appl. Polym. Mater.*, 2022, **4**, 5330−5340

49 B. M. Alameda, J. S. Murphy, B. L. Barea-López, K. D. Knox, J. D. Sisemore and D. L. Patton, Hydrolyzable Poly(β-thioether ester ketal) Thermosets via Acyclic Ketal Monomers, *Macromol. Rapid Commun.*, 2022, **2200028**, 1–8.

50 D. Guzmán, X. Ramis, X. Fernández-Francos, S. De la Flor and A. Serra, Preparation of new biobased coatings from a triglycidyl eugenol derivative through thiol-epoxy click reaction, *Prog. Org. Coatings*, 2018, **114**, 259–267.

51 T. P. Hiemenz, P.C.; Lodge, *Polymer Chemistry*, CRC Press, 2007.

52 K. Hong, Q. Sun, X. Zhang, L. Fan, T. Wu, J. Du and Y. Zhu, Fully Bio-Based High-Performance Thermosets with Closed-Loop Recyclability, *ACS Sustain. Chem. Eng.*, 2022, **10**, 1036–1046.

53 X. Xu, S. Ma, J. Wu, J. Yang, B. Wang, S. Wang, Q. Li, J. Feng, S. You and J. Zhu, High-performance, command-degradable, antibacterial Schiff base epoxy thermosets: Synthesis and properties, *J. Mater. Chem. A*, 2019, **7**, 15420–15431.

54 S. Wang, S. Ma, Q. Li, W. Yuan, B. Wang and J. Zhu, Robust, Fire-Safe, Monomer-Recovery, Highly Malleable Thermosets from Renewable Bioresources, *Macromolecules*, 2018, **51**, 8001–8012.

55 I. Itabaiana Junior, M. Avelar Do Nascimento, R. O. M. A. De Souza, A. Dufour and R. Wojcieszak, Levoglucosan: A promising platform molecule?, *Green Chem.*, 2020, **22**, 5859–5880.

56 A. S. Arya, M. T. H. Hang, M.A, Eiteman, Isolation and Characterization of Levoglucosan-Metabolizing Bacteria, *Appl. Environ. Microbiol.*, 2022, **88**, e01868-21.

57 K. Chen, X. Kuang, V. Li, G. Kang and H. J. Qi, Fabrication of tough epoxy with shape memory effects by UV-assisted direct-ink write printing, *Soft Matter*, 2018, **14**, 1879–1886.

58 D. A. Rau, J. Herzberger, T. E. Long and C. B. Williams, Ultraviolet-Assisted Direct Ink Write to Additively Manufacture All-Aromatic Polyimides, *ACS Appl. Mater. Interfaces*, 2018, **10**, 34828–34833.

59 L. Y. Zhou, Q. Gao, J. Z. Fu, Q. Y. Chen, J. P. Zhu, Y. Sun and Y. He, Multimaterial 3D Printing of Highly Stretchable Silicone Elastomers, *ACS Appl. Mater. Interfaces*, 2019, **11**, 23573–23583.

60 L. L. Lebel, B. Aissa, M. A. El Khakani and D. Therriault, Ultraviolet-assisted direct-write fabrication of carbon nanotube/polymer nanocomposite microcoils, *Adv. Mater.*, 2010, **22**, 592–596.